Graphene oxide: an all-in-one processing additive for 3D printing

Esther García-Tuñón[a,b,], Ezra Feilden[a], Han Zheng[a], Eleonora D'Elia[a], Alan Leong[a] and Eduardo Saiz[a]*

[a]Centre for Advanced Structural Ceramics, Department of Materials, Imperial College London, Royal School of Mines, Prince Consort Road, South Kensington, SW7 2BP, London, UK

[b]Materials Innovation Factory & School of Engineering, Harrison Hughes Building, Brownlow Hill, L69 3GH, University of Liverpool, Liverpool, UK

*Esther.GTunon@liverpool.ac.uk

ORCID

Esther García-Tuñón: 0000-0001-9507-4501

Keywords: 2D colloids, processing, 3D printing, complex fluids, and oscillatory rheology

Abstract

Many 3D printing technologies are based on the development of inks and pastes to build objects through droplet or filament deposition (the latter also known as continuous extrusion, robocasting or direct ink writing). Controlling and tuning rheological behaviour is key for successful manufacturing using these techniques. Different formulations have been proposed

but the search continues for approaches that are clean, flexible and robust and can be adapted to a wide range of materials. Here we show how graphene oxide (GO) enables the formulation of water-based pastes to print a wide variety of materials (polymers, ceramics and steel) using robocasting. This work combines flow and oscillatory rheology, to provide further insights into the rheological behaviour of suspensions combining GO with other materials. Graphene oxide can be used to manipulate the viscoelastic response enabling the formulation of pastes with excellent printing behaviour that combine shear thinning flow and a fast recovery of their elastic properties. These inks do not contain other additives just GO and the material of interest. As a proof of concept we demonstrate the 3D printing of additive-free graphene oxide structures, as well as polymers, ceramics and steel. Electron microscopy is used to analyse the structure of the printed materials and their mechanical properties are evaluated. Due to its amphiphilic nature and 2D structure, graphene oxide plays multiple roles behaving as a surfactant, viscosifier and binder. It stabilises suspensions of different powders, modifies the flow and viscoelasticity of materials with different chemistries, particle sizes and shapes, and binds the particles together providing green strength for manual handling. This approach enables printing complex 3D ceramic structures using robocasting with similar properties to alternative formulations, thus demonstrating the potential of using 2D colloids in materials manufacturing.

Introduction

Progress in colloidal processing is driven by the need for versatile and universal approaches to build increasingly complex parts and devices. The challenge is to manipulate the rheology of suspensions to fit specific processing techniques. Clay, the wet processing archetype, has been used for thousands of years to form ceramics, from pottery and art to advanced structural applications. Clay has a unique structure and chemistry that allows the formulation

of water-based suspensions with ideal viscoelastic behaviour for shaping, in a way that cannot be done with any other natural material. The need to replicate this behaviour and extrapolate it to other materials has driven the development of colloidal processing.[1,2] This relatively new scientific field studies the basic science behind the formulation of stable suspensions and pastes; made by combining powders with different additives (dispersants, binders, surfactants, plasticizers, viscosifiers, etc.) to emulate the shaping behaviour of natural clays. We can easily find a multitude of approaches, water or solvent based, designed to satisfy the needs for a specific material and manufacturing technique.[3-5] However, additives have their own challenges and often demand further post-processing steps. In addition, new formulations are continuously required to broaden the range of materials and to enhance the performance and flexibility of existing technologies.[1,2,6]

There are some similarities between graphene oxide (GO, also known as chemically modified graphene) and clay; both have large surface area and flake shape with a special distribution of functionalities on their geometry. Clay particles in water have different electrostatic charges on the basal plane and edges, which enables the formation of a "house of cards" arrangement and provides the plasticity required for shaping.[1] Clay is also used as an additive in suspensions of other materials to provide the right viscoelastic behaviour for processing; it has been recently used to formulate pastes for the 3D printing of composites.[7,8] Due to their anisotropic nature, aqueous suspensions of clay particles can develop a liquid crystal character.[9] On the other hand, GO, with its special combination of structure and surface chemistry, is an amphiphile. GO flakes on the basal plane are partly covered by hydrophilic functionalities (hydroxyls, carboxyl and epoxy groups); carboxyl groups are also distributed throughout the edges while some regions on the basal plane remain un-oxidized.[10] The interactions between these moieties with water and across flakes (at

pH~5 the hydroxyl functional groups in GO flakes are partly protonated[11,12] facilitating the formation of hydrogen bonds) enable the formulation of very stable, viscoelastic GO slurries, and facilitate their arrangement in a liquid crystal structure.[13,14] GO has been used in non-colloidal systems with ABS and PLA for 3D printing using fused deposition approaches.[15]GO and composites have also been 3D-printed with the aid of additives and in some cases solvents. [12,16,17] Despite the progress in the field, it is still necessary to develop flexible and robust processing approaches to bring advanced ceramics, 2D, nanoparticles, and any other materials into additive manufacturing.

This work focuses on the unique rheology of GO colloids in water, delving into their behaviour in the absence of additives; and for the first time, reporting their multiple roles enabling the processing and printing of other materials in water based systems. Here we explore clay-GO similarities and demonstrate that it is possible to use GO to create clay-like suspensions from different materials. Our findings show that graphene oxide may well be one of the most versatile processing additives available, behaving simultaneously as surfactant, rheological modifier and binder. It has the potential to simplify and enable the water-based wet processing of a wide range of materials from polymers to metals and ceramics, including highly anisotropic particles whose suspensions are usually difficult to stabilize and manipulate. The unique behaviour of graphene oxide in water can be used to tune the viscoelastic behaviour of suspensions containing particles with very different chemistries, shapes and sizes in a way that is not possible with other additives. This can be done at very low GO concentrations, with the added advantage that it can be either subsequently eliminated or retained during the post-processing steps, thus potentially adding structural or functional properties to the final part. As a proof of concept, in this work we use graphene oxide

to formulate pastes for the additive manufacturing of 3D structures made of polymers, ceramics or steel. The structure and properties of the printed parts are evaluated. These results open new, flexible and scalable possibilities for materials processing, printing and manufacturing.

Materials and Methods

Materials. GO suspensions were prepared by the exfoliation of graphite using the modified Hummers method in a custom-built reactor designed to manipulate up to 5 L of concentrated acids.[12] The suspensions were purified to remove residual salts and acids, using repeated centrifugation at 9000 rpm (Thermo Scientific Sorvall LYNX 6000 Superspeed Centrifuge) and re-dispersion in double-distilled water. Non-exfoliated particles were removed by low speed centrifugation (1000 rpm). Washing/centrifugation cycles were carried out until the particle-free supernatants had a pH ~6, typically occurring after 16 washing cycles.

GO flakes were prepared for SEM (LEO Gemini 1525) by drop-casting diluted GO solutions into silicon oxide substrates. Lateral dimensions of GO flakes were measured from SEM and optical microscopy (Axio Scope A1, Zeiss) images using ImageJ (size distribution histogram in Figure 1). Freeze-drying of a known volume of GO suspensions and weighing the dry monoliths gave an estimation of the GO content. The GO suspension and slurries were also characterised with thermo-gravimetric analysis (TGA), X-ray diffraction (XRD) and Raman spectroscopy (Figure 1). For XRD and Raman analyses the as prepared GO suspension was drop-casted on a silicon single crystal substrate and a glass slide respectively.

Alumina powders (SMA6, Baikowski, FR) with an average diameter of 0.35 μm were sieved through 100 μm to remove large agglomerates. Alumina platelets (with a lateral size of ~5 μm and thickness of ~0.3 μm, Advanced Nano Technologies Ltd., Australia) were used as provided by the supplier. Silicon carbide powders (D_{50} = 0.45 μm, UF-25, H. C. Starck, DE) were mixed with sintering aids (6 wt% alumina and 4 wt% yttria (Grade C, H. C. Starck,

DE)) in methanol for 24 h with Si_3N_4 milling media in a roll mill, followed by drying in a rotary evaporator. PVA, Poly vinyl alcohol: Mw (146,000-186,000), 99% hydrolysed, Sigma Aldrich. Steel AISI 316L micro-spheres (D_{50} = 40 μm, AISI, USA).

Rheology study of GO suspensions. The as prepared GO suspension with a concentration of 0.6 vol% was diluted 1:2 and 1:4 to evaluate the effect of flake concentration on viscosity and viscoelastic properties (Figure 2). Additionally, these suspensions were subjected to sonication using an ultrasound tip at 200W, 24kHHz, with amplitude of 60% and a pulse of 5 s for 30 min in order to break down the lateral size. Optical microscopy images (Axio Scope A1, Zeiss) were used to determine the lateral dimensions of these "small flakes" (Figure 1). These suspensions were used to evaluate the effect of flake size on rheological behaviour (Figure 2). Shear controlled flow ramps were carried out in a TA HR1 rheometer using two different geometries: 40 mm plate and 60 mm cone with a truncation gap of 59μm. Prior the oscillatory tests for the pastes we confirmed that the use of these two different geometries (cone-plate and plate-plate) during flow tests leads to consistent results for the low concentrated suspensions.

Paste preparation. GO pastes were prepared by re-dispersing freeze-dried GO powders to increase concentration (method 1); or alternatively the slurry was concentrated by water evaporation in an oil bath at 70ºC (method 2). Both approaches led to concentrated GO pastes with good behaviour for printing without the need of any other additive. A Thinky ARE-250 planetary mixer was used for both methods using several mixing cycles (2000 rpm for 2 min) in between small additions of freeze-dried GO powder or small amounts of evaporated water to guarantee a homogeneous structure within the paste. A final de-foaming step at 2200 rpm for 10 min was applied to all the samples to eliminate any remaining trapped air.

The GO suspensions obtained after graphite exfoliation/cleaning/centrifugation with a concentration of ~0.6 vol%, can be used directly as formulation base for ceramic powders, metals and polymers with a wide range of particle sizes and shapes. Including: Al_2O_3 powders and platelets, SiC powders, PVA and Steel. In order to tune viscoelasticity and flow additional freeze-dried powder was in some cases added to achieve the desired rheological behaviour. In detail, the pastes reported in this work had the following concentrations. For the alumina platelets: paste 1 with 23 vol% platelets (0.8 vol% GO (23 mg/mL)) and paste 2 with 27 vol% Al_2O_3 platelets (1.1 vol% GO (33 mg/mL), GO/Al_2O_3 ratio (3/100 in weight)). For the SiC powders: 28.4 vol% SiC with 0.4 vol% GO (10 mg/mL). For the Steel: 40.4 vol% with 0.4vol% GO (19 mg/mL). And PVA: 8.3 vol% PVA with 0.3 vol%GO (7 mg/mL). For comparative purposes suspensions of Steel and Al_2O_3 platelets and a solution of PVA in the absence of GO were also prepared to evaluate their printability and evaluate their viscoelastic responses.

Rheology of pastes. Oscillatory tests were carried out in a TA HR1 rheometer with temperature control (20 °C) and solvent trap cover using parallel plates. For concentrated pastes, the use of the plate geometry (ø = 40 mm) with a gap between 500 µm and 1mm avoids jamming of particles. The structure of the pastes and its response to different stimuli was assessed using a sequence of 5 oscillatory steps while monitoring the viscoelastic properties (G', G''). Step 1) to determine their initial internal structure and stability with a gentle oscillation at low frequency (0.5 Hz) and strain (0.5%). Step 2) to identify structure changes with a frequency sweep (fixed strain at 0.5%, frequency from 0.5– to 50 Hz). Step 3) to monitor the recovery after step 2 with a gentle oscillation at low frequency (0.5 Hz) and strain (0.5%). Step 4) to identify structure changes with strain and to measure yield stress and strain with an amplitude sweep (fixed frequency at 0.5Hz, strain from 0.1 up to 50%). Step 5) to check the recovery of the internal structure immediately after the time sweep with a gentle

oscillation at low frequency (0.5 Hz) and strain (0.5%). The waveform and Lissajous plots were monitored and recorded throughout all the steps (1 to 5) to identify non-linear events during structure changes and to track the quality of the data. The Lissajous graphs provide a visual tool to identify non-linearities: large ellipsoids that get closer to a round shape mean the behaviour is close to an ideal liquid (large area indicates that more energy is dissipated); when the ellipsoids thin up and get closer to a line, then the system is getting closer to an ideal solid.[18]

Printing. Graphene oxide based pastes were used to print 3D objects using a robotic deposition device (Robocad 3.0, 3-D inks Stillwater, OK) on a PTFE substrate, at printing speeds between 6 and 12 mm s^{-1} through 510 μm nozzles (EFD, Nordson). A 40 mm lead-in line was printed immediately before the start of each part to ensure a homogenous flow as the parts were printed, including: cylinders, grids and 40x4x3 mm^3 test bars. The temperature and humidity of the whole system was controlled by a custom built enclosure and a convection heater set to 23°C while the measured humidity varied from 70-95%.

Post-processing. GO structures were frozen in liquid nitrogen and freeze dried for 48 h (Freezone 4.5, Labconco Corporation) followed by thermal reduction at 900 °C for 1h under 10%H_2/90%Ar atmosphere. Printed parts (Alumina, SiC and Steel) were dried over 24 hours in a humidified enclosure to avoid cracking, followed by another drying step in a convection oven at 37°C. Structures built with the alumina platelets paste were sintered in a tube furnace at 1550°C under 10%H_2/90%Ar atmosphere. Once dry, SiC printed parts were isostatically pressed at 300 MPa for 1 minute at room temperature in an evacuated pouch using a Stanstead Fluid Power isostatic press and subsequently pressure less sintered under Ar atmosphere in a graphite furnace using a powder bed (to avoid loss of material due to evaporation) at 2050 °C for one hour at atmospheric pressure. All heating and cooling rates were 10 °C min^{-1}.

Characterization. The apparent density and porosity of the sintered scaffolds were measured by Archimedes' method (Sartorius, YDK01, Goettingen, Germany) in water. The microstructure and chemical composition were studied by field emission scanning electron microscopy on a LEO Gemini 1525 FEGSEM equipped with an energy dispersive spectroscopy (EDS) microprobe (INCA Sight Oxford-instruments, UK). Samples were coated with a thin Cr layer previous to the observation. X-ray diffraction (XRD) patterns were collected using a PANanalytical® XRD X'Pert Pro diffractometer operated at 40 kV and 40 mA in the 2θ range 5°–35°, with a step size of 0.0334° and a count time at each step of 100s. Raman spectroscopy was performed using a Renishaw RM2000 equipped with a 514 nm laser. Three point bending tests were carried out in a Zwick universal testing machine with a maximum load of 2 kN, using a 20 mm bottom span and a displacement rate of 0.2 mm min^{-1}. A standard 4-point probe method was used for conductivity measurements. The current was generated via a bench top PSU and kept at a constant direct current of 10 mA. Two electrodes were placed through the sample at constant distance to monitor the voltage drop through the sample. The results were derived via standard equations for electrical conductivity and resistivity in DC.

Results and Discussion

Rheology and printability of graphene oxide suspensions and pastes

Graphene oxide suspensions in water have shear thinning behaviour (Figure 1a). The viscosity and viscoelastic properties of GO suspensions in water strongly depend on their concentrations (Figure 2a),[9,19-21] which is very similar to water-clay systems.[22,23] GO suspensions with low concentrations (≤0.1 vol% GO) have liquid-like behaviour (G'<G'') with small elastic component (G' ~ 7 Pa, Figure 2b). Previous studies state that for GO aqueous dispersions, lateral size and concentration have equal influence

on viscosity.[21] However, we found that in the range of this study (i.e. lateral flake size averages varying between 16 and 44 μm, Figure 1) the lateral size has a minor effect on the viscoelastic properties for diluted suspensions, and its effect becomes negligible as flake concentration increases (Figure 2b). At concentrations above 0.1 vol%, the GO flakes form a soft solid (G'>G'') that breaks down and flows when certain yield stress is applied (Figure 3a). Increasing the GO concentration above ~2 vol% leads to a rapid rise of the solid-like component (G', Figure 3a, b) due to the formation of a well-established and organized structure (Figure 3d). We found that in these GO slurries, some of the flakes tend to roll up forming graphene oxide scrolls (Figure 3d). These changes in conformation, known as carbon nano-scrolls CNS, have been previously reported for other carbon materials.[24-26] As the slurry becomes more concentrated, GO flakes arrange forming a network,[19] similarly to a liquid crystal.[13] The increase in concentration results in a considerable increase of the elastic response with storage modulus (G') values up to 100 kPa (for 3.5 vol% GO, Figure 3b), as well as an exponential increase of the yield stress up to 2300Pa (Figure 3c). GO additive-free pastes with concentrations between ~2.5 and 3.5 vol% - prepared either by re-dispersing freeze-dried GO powders or by evaporation - display the rheological properties and structure needed for robocasting (Figures 3, 4). A comparison of the storage modulus (G', figure 3b) and yield stress (Figure 3c) of these pastes with other additive free GO suspensions in literature[16,19,20,27] confirms a consistent trend. Despite the differences in the chemistry and lateral size of the GO flakes (from 400 nm[16] and 600 nm[19] to 44 μm (this work)) and the fact that the measurements were done using different settings, the dependence of the storage modulus and the yield stress with the GO content follows a similar power law in all cases (~2.2 for the yield stress and ~2.5-3 for the storage modulus, Figure 3b, c).

Cylinders and other 3D shapes (Figure 4a, b) can be printed using these pastes. Thanks to their shear thinning behaviour, they easily flow through small nozzles and quickly recover once the shear eases off, retaining the shape once printed and supporting the layers on top (Figure 4a, b). A sequence of oscillatory stimuli in the rheometer provides insights into the structure, stability and response to frequency and strain for the 3 vol% GO (76 mg/mL) paste (Figure 4). Its solid-like (G' > G'') structure is very stable within the LVR at all times except for the transition to liquid-like at strains of 16%. In more detail, during step 1 the sinusoidal signal is free of background noise and no non-linear effects can be detected in the Lissajous graph, which has a clear ellipsoid shape. As frequency increases in step 2, a slight increase of the liquid-like component is detected (see phase between sinusoidal signals and Lissajous curve, Figure 4c), but still the solid-like dominates with linear behaviour. The time sweep (step 3) shows how the paste immediately recovers its initial structure once the frequency is reduced to 0.5 Hz. During the amplitude sweep (step 4), as strain increases the structure starts to break down and non-linear effects are detected in the sinusoidal signals and Lissajous graphs. The loss of structure and transition from solid-like to liquid-like takes place at a yield stress of 254 Pa and strain of 16%, corresponding with the transition to non-linear behaviour. This illustrates the structural changes of the paste as it travels through the nozzle during the printing process. The final time sweep (step 5) shows how the GO network quickly recovers (the signals and Lissajous curves correspond to the first point measured in this region). Although there is a slight increase of G'' comparing with initial values (also a bigger phase lag and a larger area within the Lissajous plot), G' and G'' values are in the same order of magnitude as in the initial step. This illustrates the rebuild of the structure that recovers its initial elasticity with G' values >10,000, facilitating the printing of filaments that retain their shape (Figure 5a), are self-supporting and strong enough to support the layers on top.

After post-processing the 3D printed GO parts have internal microstructure (Figure 5b, c) and functional properties similar to those made using alternative formulations (based in pH responsive surfactants (BCS)[12] and hydrogels (F127)) and other assembling approaches besides 3D printing, including freezing and emulsion templating approaches of graphene, reduced graphene oxide and other carbon materials (Figure 5e). [16,28-37] Microstructural analyses reveal how at the micro scale the flakes arrange in a porous 3D network (Figure 5b) and evidence the formation of graphene oxide scrolls bridges across flakes (Figure 5c). The scroll formation is more noticeable for additive free GO slurries prepared by water evaporation (Figure 5c). Raman spectroscopy on reduced flakes at 250 °C and 900 °C confirm the increase of the Id/Ig ratio (figure 5d)[38]. Printed cylinders after reduction display the expected values of density and electrical conductivity (Figure 5e).

Graphene oxide as printing additive for a polymer solution (PVA)

Besides additive-free printable and self-supporting GO pastes, it is also possible to design GO-based printable formulations of a wide range of materials with different chemistries, shapes and particle sizes. These pastes do not contain any further additives, only water, graphene oxide flakes and the material of interest. We have demonstrated the use of this approach with solutions (such as PVA polymers poly vinyl alcohol, Figure 6), and particulate systems such as ceramic powders (SiC and Al_2O_3) and platelets, and even steel micro spheres. Due to its two dimensional nature and high surface area, the addition of GO at low concentration ranges (between 0.1 and 1 vol%) to other materials changes their rheological behaviour, facilitating the viscoelasticity required for the printing process. All the pastes are shear thinning and have viscoelastic behaviour with G' dominating (i.e. solid like behaviour), however each of them has a unique viscoelastic fingerprint that depends on the intrinsic properties of the filler. PVA solutions (8 vol%) on their own do not exhibit adequate

viscoelastic properties for robocasting (supporting information, Figures S1 & S2). PVA solutions have liquid-like behaviour with low values of G' (< 1 Pa, Figure S2) and time-dependent behaviour,[39] which is incompatible with 3D printing by continuous extrusion. But small additions of GO (0.3 vol%) shift their viscoelastic response, forming a printable gel with G' values over 1000 Pa that does not break down under frequency or amplitude sweeps (Figure 6, S2). For all the oscillations performed on this paste, the sinusoidal signal is free of background noise and no non-linear effects can be detected in the Lissajous curves, which have a clear ellipsoid shape. At strains ~20% its structure becomes less elastic (G' values only drop slightly) but does not break down; it has a true-gel behaviour. The final time sweep (step 5) shows how this system quickly recovers its initial structure with G' and G'' values that remain with same order of magnitude.

3D printing of particulate systems using GO as printing additive

The same process can be used for particles with different chemistries, shapes and sizes. For example, GO also aids the processing and printing of steel micro-spheres, which cannot be stabilised or printed without the aid of GO (supporting information, Figure S1, S3 & S4). The smooth spherical shape and wide size distribution of these steel particles (Figure 7) facilitate very efficient packing, leading to pastes that can reach solid loadings above 40 vol% with only 0.4 vol% GO. Oscillatory tests show that this paste has a very stable structure within the LVR with high G' values (supporting information, Figure S3). The structure breaks down leading to a non-linear liquid-like system at strains of ≈ 23%, but quickly recovers its linearity and reaches G' values of 120 kPa when the strain is reduced to 0.5% (Figure S3). These G' values are high enough to facilitate the printing of self-supporting 3D objects (Figure 7a). However an important limiting factor for the extrusion of this paste is the

sedimentation of the large and heavy steel spheres that takes place within the syringe barrel, resulting on water segregation and clogging the nozzle. Reducing solids loading, increasing GO content or alternatively using of smaller steel particles could solve this limitation. SEM analysis reveals the sphere arrangement on the external surface of the filament (Figure 7b), which corresponds to the laminar flow region in the walls of the nozzle. Close up images in a cross section illustrate the strong interaction between the GO flakes and the surface of the steel spheres. The GO flakes form an envelope around the particles, binding them together (Figure 7c-e).

Complex ceramic structures can be built applying the same principles to ceramic powders such as alumina (Figures 8-10) and silicon carbide (Figure 11). In this work we used this approach for Al_2O_3 with different shapes, such as particles and platelets, and SiC powders with different sizes, but similar principles would apply to any other ceramic material. As an example, a suspension of only alumina platelets in water (without GO or any other additive) has a very unstable viscoelastic response with liquid like behaviour (supporting information, Figures S1, S5 & S6), which proves the key role of GO stabilising the ceramic particles as well as printing aid. Our findings suggest that different particle sizes (i.e. different specific surfaces) and shapes require slightly different amounts of added GO to achieve the right texture to be printable. Pastes of Al_2O_3 platelets can be prepared with a wide range of particle/GO ratios but the best printing behaviour was found for a mixture of ~28 vol% platelets with 1.1 vol% GO (Figures 8, 9, S5, S6). It is possible to use this paste to make bulk shapes, grids and even free-standing micro-pillars printed vertically using robocasting (Figure 9b). The structure of this system is solid-like within the linear region (Figure S5). Strains of ~4% break down the structure leading to a non-linear transition (supporting information, Figure S5), which illustrates the viscoelasticity changes as the paste shear

thins on its way through the nozzle. The extrusion process also defines the arrangement of platelets and the internal architecture of the printed objects. Cross-sections and lateral views of printed filaments (Figure 8c, d respectively) show how the platelets arrange on the outside edge forming a wall, while the inside has a mixture of domains (Figure 8c, d respectively). Platelets arrange parallel to each other inside a domain but the different domains seem to be randomly oriented with respect to each other. This arrangement is dictated by the extrusion profile, which depends on the viscosity (that changes non linearly across the cross section due to the shear profile), printing speed, and tip diameter and length.[40] Upon close-up observation (Figure 9), GO flakes appear to have a strong interaction with the platelets, spreading over and across the surfaces of multiple Al_2O_3 platelets, binding them together and forming bridges across them (Figure 9). The structure and multifunctional chemistry of GO (with hydroxyl, carboxyl, epoxy functional groups and hydrophobic islands in the basal plane) facilitate multiple interactions due to the affinity of these functional groups with the oxide surfaces. We propose that at this pH range (pastes exhibit pH values between 5 and 6), non-covalent interactions such as hydrogen bonds (flake to flake and flake to particle) may be playing an important role.[12,41] The structures built using the platelet/GO paste exhibit good handling strength once dry and before sintering. The GO/platelet interactions are strong enough to hold the structure together without particle debris. After sintering, these structures have an average porosity of 60% with only 2% closed pores (Figure 10a-c). Sintering in a reducing atmosphere at 1550 °C in a tube furnace does not prevent the full burnout of GO, highly likely due to the length of the thermal treatment and the high porosity of the sample. Other structures made with the same alumina platelets and F127 (similarly to previous work on this field[42]) but without GO do not sinter and display debris when handled

manually. The structures made with GO display good handling strength once sintered, suggesting that it is also playing a role as sintering aid (Figure 10d, e). XRD analysis after sintering confirms that Al_2O_3 is the only crystalline phase, and no carbon bands were identified with Raman spectroscopy. These porous architectures would be an ideal scaffold for the fabrication of composites (Figure 10).

GO can also aid the processing of non-oxide ceramics; SiC is used here as model system. We found that the response of SiC-GO pastes during the oscillatory tests is less stable than the other systems studied in this work (supporting information, Figure S7). G' and G'' change over time, the sinusoidal response displays background noise and non-linear effects take place throughout the oscillatory tests (Figure S7). The behaviour of this sample is very sensitive to its history, showing important structural changes as the sequence of oscillatory stimuli takes place. This is highly likely due to the irregular shape and small size (D_{50} = 0.45 μm) of the SiC particles (Figure 11). The interactions between GO and the non-oxide surfaces might be also playing a role on this more complex and sensitive viscoelastic response. However, further analyses on these aspects currently fall outside of the scope of this work. Despite its sensitive stability and non-linear behaviour, this paste displays adequate printing behaviour. The network breaks down and flows through the nozzle due to the shear-thinning behaviour, and re-builds with enough stiffness (G' > G'', and G' in the order of 5kPa) to print bulk 3D objects, for example bars for mechanical testing, cylinders and lattices (Figures 11, 12). Once dry, SiC 3D printed bars have strengths of ~1 MPa measured in 3-point bending, proving that GO is also acting as a binder of SiC surfaces. During the mechanical tests of these green structures, some GO flakes were bridging across the cracks, which suggests that an additional reinforcement mechanisms might be taking place. However, the visual inspection of fractured surfaces in the SEM did not provide

clear insights on the SiC/GO interactions (Figure 11c). Sintered SiC bars (2050 ºC for 2 hours) have a final density of 3.21 g/cm^3 (96.4% of the theoretical, Figure 12) and bending strengths of ~212 MPa. These properties match with those for SiC parts printed using hydrogel based (F127) formulations and subjected to the same sintering conditions.[42] No carbon phases were detected with Raman on sintered samples. XRD analyses indicate that SiC is the only crystalline phase.

Summarising, all the GO based systems formulated in this work display non-Newtonian shear thinning behaviour and viscoelastic response with the elastic component dominating (G' > G''). For comparative purposes the viscoelastic fingerprints (frequency and amplitude sweeps) for all of them are compiled in Figure 13. Despite the similarities, each system has a unique viscoelastic fingerprint (Figure 13 a, b). Their individual response is intimately related to the solid loading (which is defined by the intrinsic properties of the filler such as size, specific surface and density) and highly likely due to the different nature of the interactions at the GO/material interfaces. In general, larger particles with smooth surfaces (steel and alumina platelets) allow higher solid contents due to the smaller specific surface area. This results in pastes with more stable structures, linear behaviour and larger values for G' (Figure 13c). On the other hand, small anisotropic non-oxide particles (as SiC) lead to more complex internal structures with non-linear behaviour. This might be due to the contribution of different factors: as the friction between small and irregular particles with a narrow distribution that limit the solid loading, packing and flow; and different interactions at the GO/SiC interface. Despite these differences, all the experiments carried out with these very diverse materials confirm that the GO flakes are simultaneously playing different roles: 1) as surfactant, stabilizing particle suspensions of oxide (Al_2O_3) and non-oxide (SiC) ceramics and steel; 2) as viscosifier,

providing the rheological behaviour needed for robocasting; and 3) as binder, bonding the particles forming a stable structure after drying, providing printed shapes that are stable and easy to handle manually once dry.

Using GO instead of other currently available formulations in literature (for example hydrogels (F127), pH responsive surfactants, clays or PEI) provides key advantages for materials manufacturing: simplicity, versatility, flexibility, scalability and robustness. Here, GO is the only additive while other formulations in literature require multiple ingredients and even the use of solvents.[16,17,43] GO's multifunctional surface chemistry plays complementary roles as processing enabler for different materials. Unlike clay (that provides electrostatic interactions) GO can establish hydrophobic, steric and non-covalent (i.e. hydrogen bonds) interactions with other materials. Due to its large surface area, very small amounts of GO can completely shift the viscoelastic response, while for example the standard concentration for F127 hydrogels is ~25wt%,[42,44] which can become a problem during post-processing steps. For example, the burnout of large amounts of volatile organics restricts the use of spark plasma sintering (SPS) for structures made with F127 formulations. Additionaly, thanks to its 2D structure, GO flakes (unlike clay particles) can twist, bend and roll up establishing multiple interactions in a 3D network. And lastly, GO colloids provide formulations with robust viscoelastic responses that are independent of external stimuli; on the contrary F127, pH responsive surfactants and PEI are sensitive to temperature or pH.[42,43]

Conclusions

We have shown that there are key similarities between graphene oxide and clay. Both exhibit a flake-like shape with different functionalities on their edges and faces that

result in the formation of particle networks connected by electrostatic interactions for clay, and non-covalent interactions for GO. As a result, like for clay, graphene oxide aids the formulation of pastes for wet processing, providing the right viscoelastic response to a very wide range of materials, with different chemistries, particle morphologies (from particles, platelets and fibres to micro spheres) and sizes (from nano to tens of microns). Graphene oxide is an all-in-one additive, acting as a surfactant, viscosifier, printing aid and binder; leading to formulations containing only three components, graphene oxide, water and the material of interest. After printing graphene oxide can be eliminated (e.g. by a thermal treatment in an oxidizing atmosphere) or could be retained to potentially add functionality to the final materials, by designing post-processing steps to facilitate in-situ reduction, for example spark plasma sintering.

While it could be argued that graphene based materials are very expensive additives, this is only true for pristine graphene or CVD graphene. Graphene oxide – exfoliated graphite – can be produced on a large scale and only small amounts are required for this application. This opens up multiple possibilities for materials manufacturing. In particular for robocasting of complex structures and composites, as well as new processing approaches for other traditional and modern techniques, for example casting, injection, and roll-to-roll processes.

ACKNOWLEDGEMENTS

EGT and ES would like to acknowledge the EPSRC Grant graphene 3D networks (EP/K01658X/1) and Manufacture Using Advanced Powder Processes (MAPP EP/P006566/1). EF would like to acknowledge the CASC (Centre for Advanced Structural Ceramics) industrial consortium. ED would like to acknowledge funding from the Defence

Advanced Research Projects Agency (DARPA), “Bio-inspired self-healing materials based on ceramic-polyurethane hybrid composites”. AL would like to acknowledge PETRONAS (Graphene Composites for Pipelines).

SUPPORTING INFORMATION

Stability of steel particles in water (Figure S1); printability of PVA, Al_2O_3 and steel in water without GO (Figure S1); additional information and rheological fingerprints with and without GO for PVA (Figure S2), steel (Figures S3, S4), Al_2O_3 platelets (Figures S5, S6) and SiC (S7).

ABBREVIATIONS

GO, graphene oxide; PVA, polyvinyl alcohol; CMG, chemically modified graphene; rGO, reduced graphene oxide; PEI, poly(ethylenimine)

REFERENCES

(1) Lewis, J. A. Colloidal Processing of Ceramics. *J. Am. Ceram. Soc.* **2000**, *83* (10), 2341–2359.
(2) Greil, P. Advanced Engineering Ceramics. *Adv. Mat.* **2002,** *4* (5), 247–254.
(3) Ahn, B. Y.; Duoss, E. B.; Motala, M. J.; Guo, X.; Park, S. I.; Xiong, Y.; Yoon, J.; Nuzzo, R. G.; Rogers, J. A.; Lewis, J. A. Omnidirectional Printing of Flexible, Stretchable, and Spanning Silver Microelectrodes. *Science* **2009**, *323* (5921), 1590–1593.
(4) Smay, J. E.; Gratson, G. M.; Shepherd, R. F.; Cesarano, J.; Lewis, J. A. Directed Colloidal Assembly of 3D Periodic Structures. *Adv. Mat.* **2002**, *14* (18), 1279–1283.
(5) Heule, M.; Vuillemin, S.; Gauckler, L. J. Powder-Based Ceramic Meso- and Microscale Fabrication Processes. *Adv. Mat.* **2003**, *15* (15), 1237–1245.
(6) Evans, J. Seventy Ways to Make Ceramics. *J. Eur. Ceram. Soc.* **2008**, *28* (7), 1421–1432.
(7) Compton, B. G.; Lewis, J. A. 3D-Printing of Lightweight Cellular Composites. *Adv. Mat.* **2014**, *26* (34), 5930–5935.
(8) Sydney Gladman, A.; Matsumoto, E. A.; Nuzzo, R. G.; Mahadevan, L.; Lewis, J. A. Biomimetic 4D Printing. *Nat. Mater.* **2016**, *15* (4), 413–418.
(9) Michot, L. J.; Bihannic, I.; Maddi, S. Liquid–Crystalline Aqueous Clay Suspensions; PNAS **2006**, 103, 16101–16104.
(10) Kim, F.; Cote, L. J.; Huang, J. Graphene Oxide: Surface Activity and Two-Dimensional Assembly. *Adv. Mat.* **2010**, *22* (17), 1954–1958.
(11) Konkena, B.; Vasudevan, S. Understanding Aqueous Dispersibility of Graphene Oxide and Reduced Graphene Oxide Through P KaMeasurements. *J. Phys. Chem. Lett.* **2012**, *3* (7), 867–872.
(12) García-Tuñón, E.; Barg, S.; Franco, J.; Bell, R.; D'Elia, E.; Maher, R. C.; Guitián, F.; Saiz, E. Printing in Three Dimensions with Graphene. *Adv. Mat.* **2015**, *27* (10), 1688–1693.
(13) Xu, Z.; Gao, C. Aqueous Liquid Crystals of Graphene Oxide. *ACS Nano* **2011**, *5* (4), 2908–2915.
(14) Liu, Y.; Xu, Z.; Gao, W.; Cheng, Z.; Gao, C. Graphene and Other 2D Colloids: Liquid

Crystals and Macroscopic Fibers. *Adv. Mat.* **2017**, 1606794.
(15) Wei, X.; Li, D.; Jiang, W.; Gu, Z.; Wang, X.; Zhang, Z.; Sun, Z. 3D Printable Graphene Composite. *Scientific Reports* **2015**, 1–7.
(16) Zhu, C.; Han, T.; Duoss, E. B.; Golobic, A. M. Highly Compressible 3D Periodic Graphene Aerogel Microlattices. *Nature* **2015**.
(17) Román-Manso, B.; Figueiredo, F. M.; Achiaga, B.; Barea, R.; Pérez-Coll, D.; Morelos-Gómez, A.; Terrones, M.; Osendi, M. I.; Belmonte, M.; Miranzo, P. Electrically Functional 3D-Architectured Graphene/SiC Composites. *Carbon* **2016**, *100*, 318–328.
(18) Hyun, K.; Wilhelm, M.; Klein, C. O.; Cho, K. S.; Nam, J. G.; Ahn, K. H.; Lee, S. J.; Ewoldt, R. H.; McKinley, G. H. A Review of Nonlinear Oscillatory Shear Tests: Analysis and Application of Large Amplitude Oscillatory Shear (LAOS). *Prog. Polym. Sci.* **2011**, *36* (12), 1697–1753.
(19) Vallés, C.; Young, R. J.; Lomax, D. J.; Kinloch, I. A. The Rheological Behaviour of Concentrated Dispersions of Graphene Oxide. *J. Mater. Sci.* **2014**, *49* (18), 6311–6320.
(20) Naficy, S.; Jalili, R.; Aboutalebi, S. H.; Gorkin, R. A., III; Konstantinov, K.; Innis, P. C.; Spinks, G. M.; Poulin, P.; Wallace, G. G. Graphene Oxide Dispersions: Tuning Rheology to Enable Fabrication. *Mater. Horiz.* **2014**, *1* (3), 326–331.
(21) Bao, C.; Zhang, H.; Wilkie, C. A.; Bi, S.; Tang, X. Z.; Wu, J.; Yang, J. On the Dispersion Systems of Graphene-Like Two-Dimensional Materials: From Fundamental Laws to Engineering Guidelines. *Carbon* **2016**, *107* (C), 774–782.
(22) Coussot, P. Structural Similarity and Transition From Newtonian to Non-Newtonian Behavior for Clay-Water Suspensions. *Phys. Rev. Lett.* **1995**, *74* (20), 3971-3974.
(23) Mourchid, A.; Lecolier, E.; Van Damme, H.; Levitz, P. On Viscoelastic, Birefringent, and Swelling Properties of Laponite Clay Suspensions: Revisited Phase Diagram. *Langmuir* **1998**, *14* (17), 4718–4723.
(24) Dong, X.; Xing, G.; Chan-Park, M. B.; Shi, W.; Xiao, N.; Wang, J.; Yan, Q.; Sum, T. C.; Huang, W.; Chen, P. The Formation of a Carbon Nanotube–Graphene Oxide Core–Shell Structure and Its Possible Applications. *Carbon* **2011**, *49* (15), 5071–5078.
(25) Liu, Z.; Xue, Q.; Tao, Y.; Li, X.; Wu, T.; Jin, Y.; Zhang, Z. 2 Modeling and Methods. *Phys. Chem. Chem. Phys.* **2015**, *17*, 3441–3450.
(26) Jayasena, B.; Subbiah, S.; Reddy, C. D. Formation of Carbon Nanoscrolls During Wedge-Based Mechanical Exfoliation of HOPG. *J. Micro Nano-Manuf.* **2014**, *2* (1), 011003.
(27) Li, W.; Li, Y.; Su, M.; An, B.; Liu, J.; Su, D.; Li, L.; Li, F.; Song, Y. Printing Assembly and Structural Regulation of Graphene Towards Three-Dimensional Flexible Micro-Supercapacitors. *J. Mater. Chem. A* **2017**, *44*, 3639.
(28) Barg, S.; Perez, F. M.; do V Pereira, P.; Na, N.; Maher, R.; Garcia-Tunon, E.; Agnoli, S.; Eslava, S.; Mattevi, C.; Saiz, E. Mesoscale Assembly of Chemically Modified Graphene Into Complex Cellular Networks. *Nat. Commun.* **2014**, *5*, 1–10.
(29) Guan, L.-Z.; Gao, J.-F.; Pei, Y.-B.; Zhao, L.; Gong, L.-X.; Wan, Y.-J.; Zhou, H.; Zheng, N.; Du, X.-S.; Wu, L.-B.; Jiang, J.-X.; Liu, H.-Y.; Tang, L.-C.; Mai, Y.-W. Silane Bonded Graphene Aerogels with Tunable Functionality and Reversible Compressibility. *Carbon* **2016**, *107* (C), 573–582.
(30) Lin, Y.; Liu, F.; Casano, G.; Bhavsar, R.; Kinloch, I. A.; Derby, B. Pristine Graphene Aerogels by Room-Temperature Freeze Gelation. *Adv. Mat.* **2016**, *28* (36), 7993–8000.
(31) Zou, J.; Liu, J.; Karakoti, A. S.; Kumar, A.; Joung, D.; Li, Q.; Khondaker, S. I.; Seal, S.; Zhai, L. Ultralight Multiwalled Carbon Nanotube Aerogel. *ACS Nano* **2010**, *4* (12), 7293–7302.
(32) Zhang, X.; Sui, Z.; Xu, B.; Yue, S.; Luo, Y.; Zhan, W.; Liu, B. Mechanically Strong and Highly Conductive Graphene Aerogel and Its Use as Electrodes for Electrochemical Power Sources. *J. Mat. Chem.* **2011**, *21* (18), 6494–6497.
(33) Worsley, M. A.; Kucheyev, S. O.; Satcher, J. H., Jr. Mechanically Robust and Electrically Conductive Carbon Nanotube Foams. *Appl. Phys. Lett.* **2009**, No 94.
(34) Chen, Z.; Ren, W.; Gao, L.; Liu, B.; Pei, S.; Cheng, H.-M. Three-Dimensional Flexible and Conductive Interconnected Graphene Networks Grown by Chemical Vapour

Deposition. *Nat. Mater.* **2011**, *10* (6), 424–428.
(35) Qiu, L.; Liu, J. Z.; Chang, S.; Wu, Y.; Li, D. Biomimetic Superelastic Graphene-Based Cellular Monoliths. *Nat. Commun.* **2012**, *3*.
(36) la Osa, de, G.; Pérez-Coll, D.; Miranzo, P.; Osendi, M. I.; Belmonte, M. Printing of Graphene Nanoplatelets Into Highly Electrically Conductive Three-Dimensional Porous Macrostructures. *Chem. Mater.* **2016**, *28* (17), 6321–6328.
(37) Qian, Y.; Ismail, I. M.; Stein, A. Ultralight, High-Surface-Area, Multifunctional Graphene-Based Aerogels From Self-Assembly of Graphene Oxide and Resol. *Carbon* **2014**, *68* (C), 221–231.
(38) Cançado, L. G.; Jorio, A.; Ferreira, E. H. M.; Stavale, F.; Achete, C. A.; Capaz, R. B.; Moutinho, M. V. O.; Lombardo, A.; Kulmala, T.; Ferrari, A. C. Quantifying Defects in Graphene via Raman Spectroscopy at Different Excitation Energies. *Nano Letters*, **2011**, 3190–3196.
(39) Gao, H.; He, J.; Yang, R.; Yang, L. Characteristic Rheological Features of High Concentration PVA Solutions in Water with Different Degrees of Polymerization. *J. Appl. Polym. Sci.* **2010**, *116*, 2734–2741.
(40) Feilden, E.; Ferraro, C.; Giuliani, F.; Vandeperre, L.; Saiz, E. Progress in Novel and Unexpected Areas. *Mat. Today* **2016**, *19* (9).
(41) García-Tuñón, E.; Machado, G. C.; Schneider, M.; Barg, S.; Bell, R. V.; Saiz, E. Complex Ceramic Architectures by Directed Assembly of "Responsive"Particles. *J. Eur. Ceram. Soc.* **2017**, *37* (1), 199–211.
(42) Feilden, E.; García-Tuñón, E.; Giuliani, F.; Saiz, E.; Vandeperre, L. Journal of the European Ceramic Society. *J. Eur. Ceram. Soc.* **2016**, *36* (10), 2525–2533.
(43) Lewis, J. A.; Smay, J. E.; Stuecker, J.; Cesarano, J. Direct Ink Writing of Three-Dimensional Ceramic Structures. *J. Am. Ceram. Soc.* **2006**, *89* (12), 3599–3609.
(44) Goyos-Ball, L.; García-Tuñon, D. E.; Fernández-García, E.; Díaz, R.; Fernández, A.; Prado, C.; Saiz, E.; Torrecillas, R. Journal of the European Ceramic Society. *J. Eur. Ceram. Soc.* **2017**, *37* (9), 3151–3158.
(45) Marcano, D. C.; Kosynkin, D. V.; Berlin, J. M.; Sinitskii, A.; Sun, Z.; Slesarev, A.; Alemany, L. B.; Lu, W.; Tour, J. M. Improved Synthesis of Graphene Oxide. *ACS Nano* **2010**, *4* (8), 4806–4814.

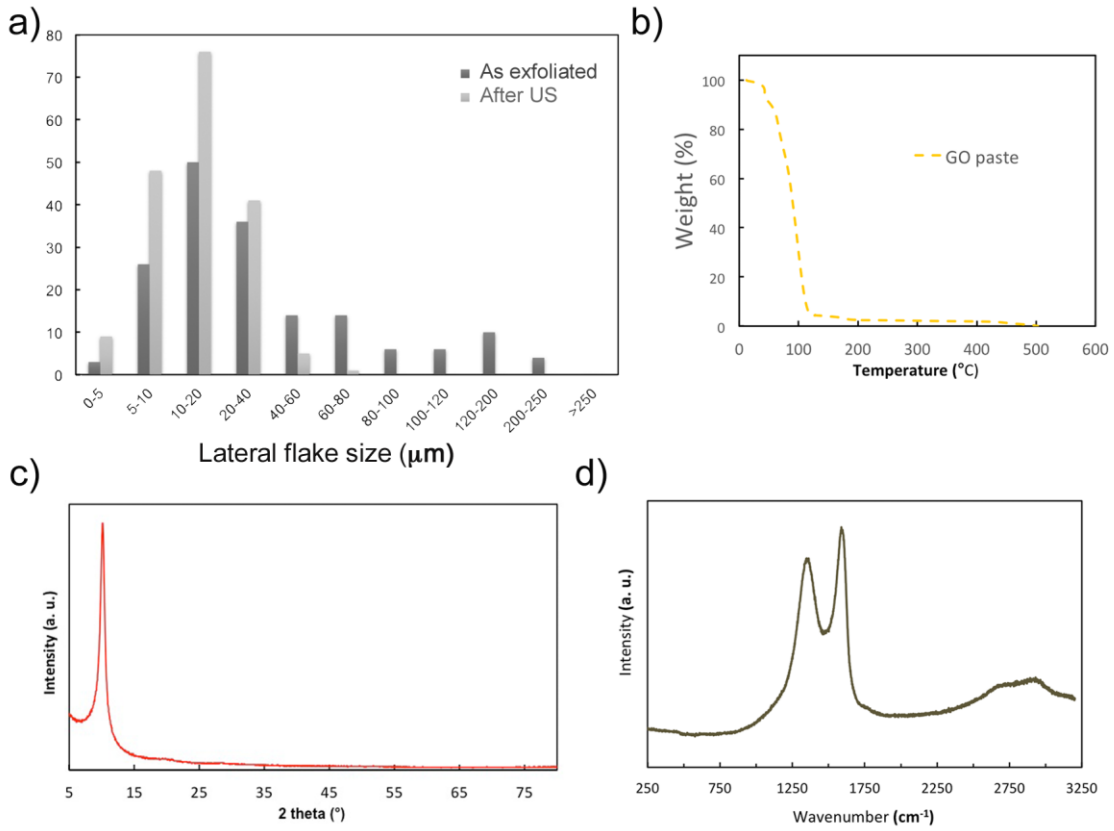

Figure 1. GO characterization: a) Lateral flake size distribution obtained from >100 flakes from SEM and optical microscopy images using ImageJ. As exfoliated the average flake size is 44 µm, breaking down to an average of 16 µm after ultra sounds. b) Thermo-gravimetric analysis (of a concentrated GO slurry carried out in air) shows the water loss (95.5 wt%) up to 100 °C, and no residues at 500 °C as all the carbon has been burnt out. **c**) X-ray diffraction analysis of a suspension droplet let dry in air, showing the characteristic peak for GO at 2theta ≈ 10°[45]. d) Raman spectroscopy analysis performed on a dry droplet of GO suspension, showing its characteristic bands (D at 1361 cm^{-1}, G at 1598 cm^{-1}, and a small shoulder around the 2D band at 2730 cm^{-1})[38].

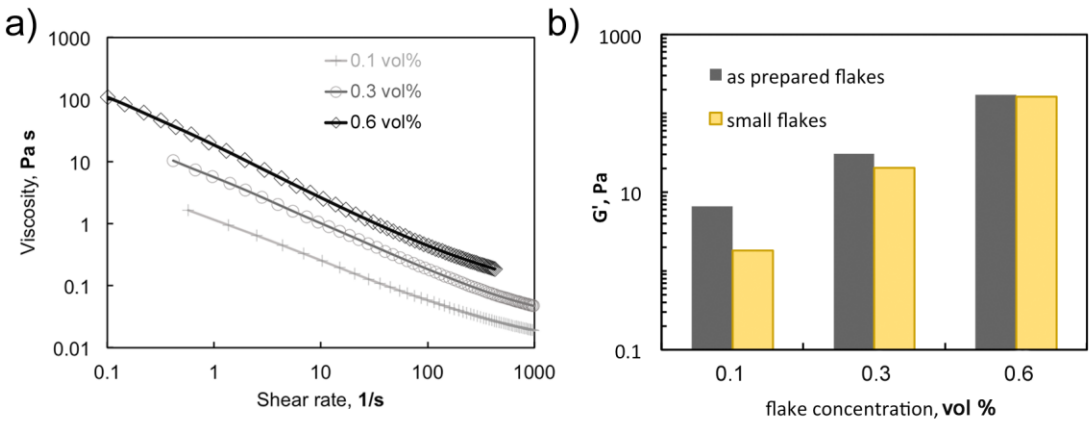

Figure 2. Flow behaviour and viscoelastic properties (G', storage modulus) of GO oxide suspensions and pastes with increasing concentrations of GO flakes in the absence of additives. a) The flow ramps show how the viscosity rapidly increases for diluted GO suspensions in water with concentrations between 0.1 and 0.6 vol%. b) Histogram showing the effect of flake size (as prepared 44 μm vs. after ultrasounds 16 μm) on the viscoelastic response of GO diluted suspensions with flakes with different lateral flake sizes and distributions (Figure 1). There is a slight drop of the storage modulus (G') for a 0.1 vol% suspension prepared with small flakes, but as GO concentration increases the effect of flake size on viscoelastic properties becomes insignificant. GO solutions with 0.6 vol% solids made with different flake sizes have similar values of G'.

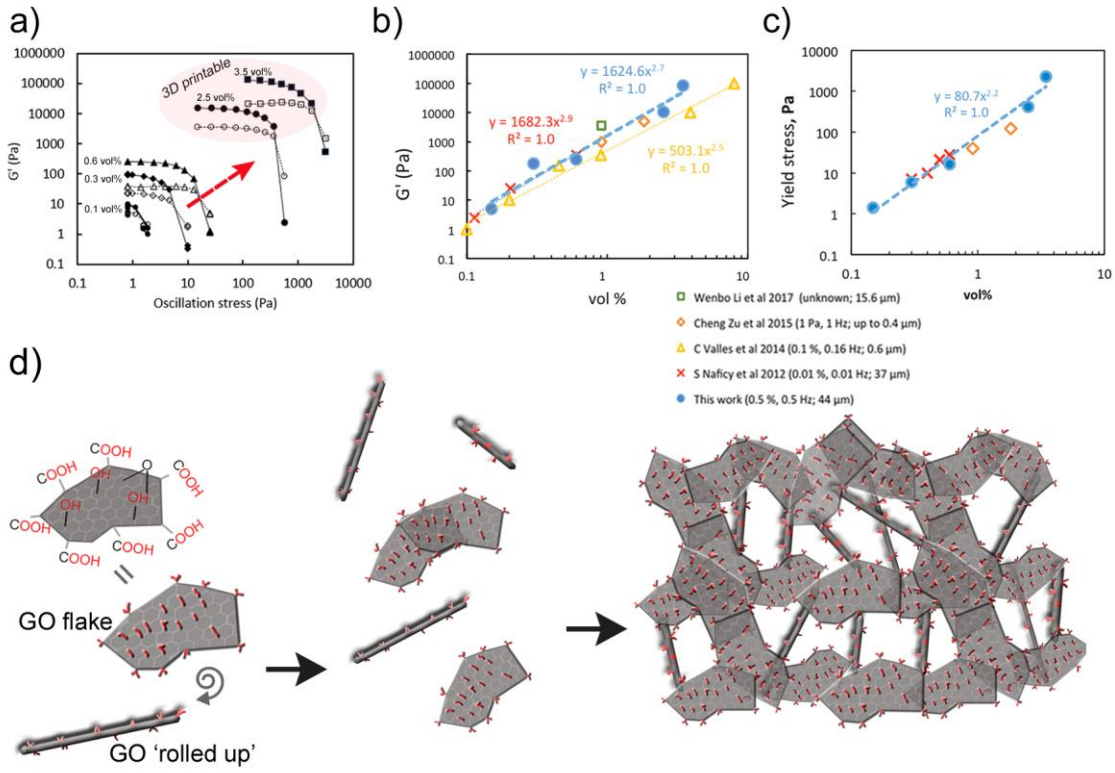

Figure 3. Viscoelastic properties for GO suspensions and pastes: fingerprints (a), and effect of GO concentration on G' (storage modulus, b) and yield stress (c). The more concentrated systems are printable (labelled 3D-printable in a). The storage modulus (b) and yield stress (c) increase with flake concentration following a power law, in agreement with existing literature on the subject.[16,19,20,27] d) Schematic showing the proposed assembly of GO flakes in water as concentration increases. Some of the GO flakes roll up forming graphene oxide scrolls; both assemble into a 3D liquid crystal structure with a strong elastic response (a).

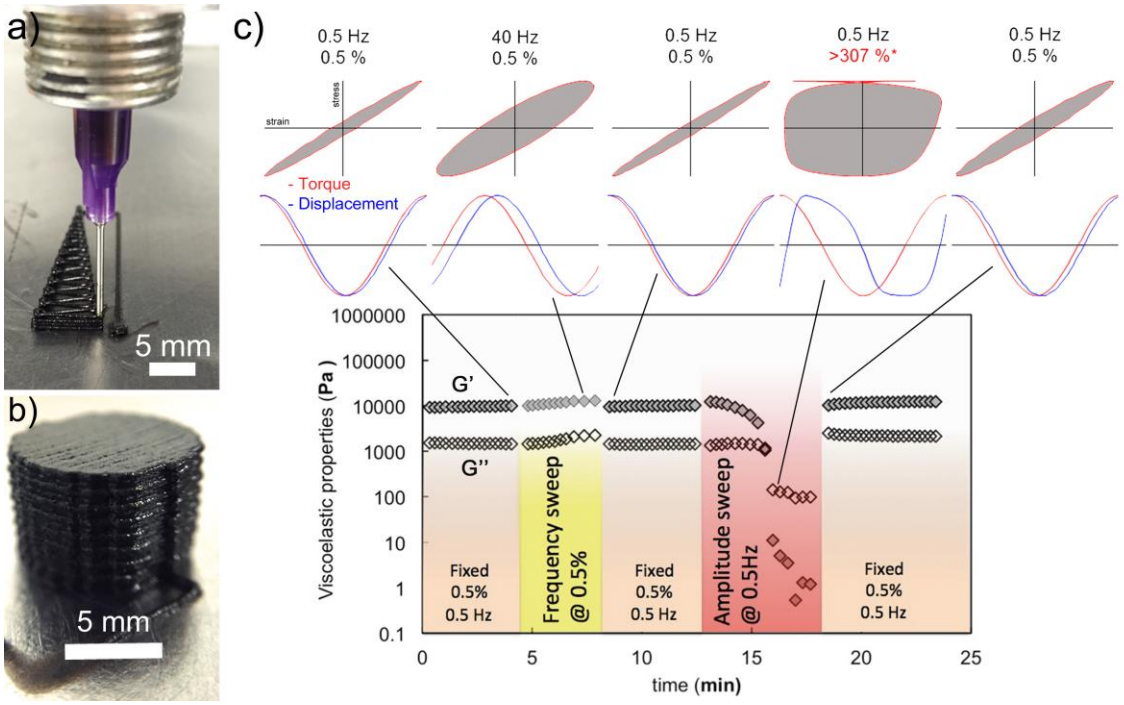

Figure 4. Printed structures and oscillatory rheology of additive free GO pastes. a) Image of a structure printed to test the stiffness of the filaments across spans with increasing lengths. The filaments retain their shape well across spans up to 15 mm during printing, but they tend to deflect during drying for the larger gaps. b) 3D printed cylinder made for bulk characterization of the paste after post-processing (density and electrical conductivity). c) Evolution of viscoelastic fingerprints for a GO paste without additives (3 vol% GO in water, which corresponds to 76 mg/mL). Including the waveform and Lissajous plots for some of the points. These graphs illustrate structure changes with frequency and strain. Frequency slightly increases the liquid-like behaviour (frequency seep). The GO networks breaks down and flows with a liquid-like behaviour during the amplitude sweep.

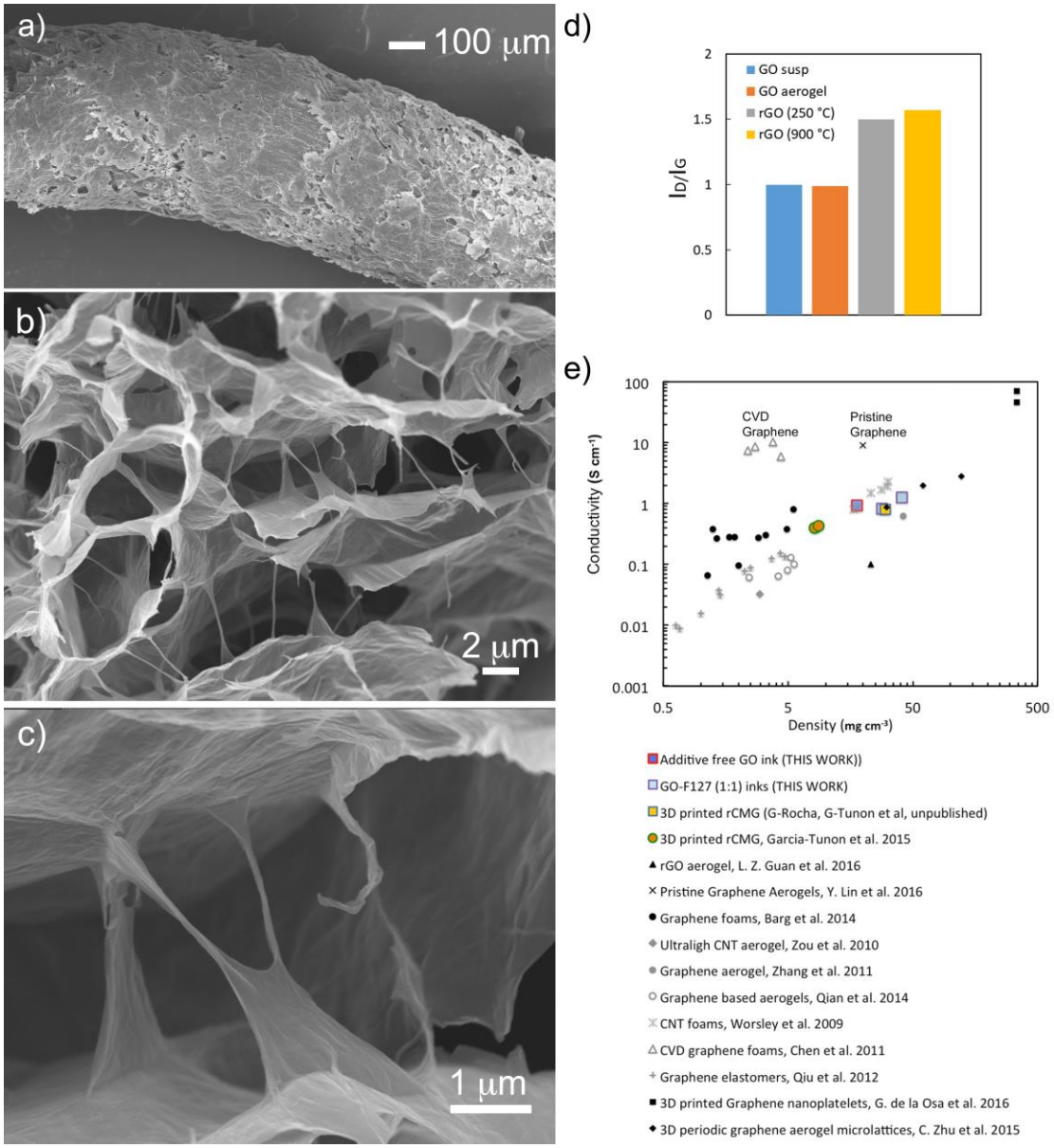

Figure 5. a) External surface of additive free printed filaments of GO. b) Image of the internal microstructure showing the formation of GO scrolls interconnecting the 3D network, in more detail at higher magnification (c). d) Histogram showing the evolution of the I_D/I_G ratio after thermal treatment. Before any thermal treatment, both GO suspension and also the aerogel have wide D and G peaks with similar intensity. After thermal reduction (at 250 °C and 900 °C) the I_D/I_G ratio increases confirming the recrystallization and reduction of GO to rGO. e) Graph comparing the electrical conductivity of 3D printed cylinders using different water based formulations (responsive surfactants, hydrogel base F127 and no additives (NA)) as well as with other structures found in the literature made following different methods.[12,16,28-37]

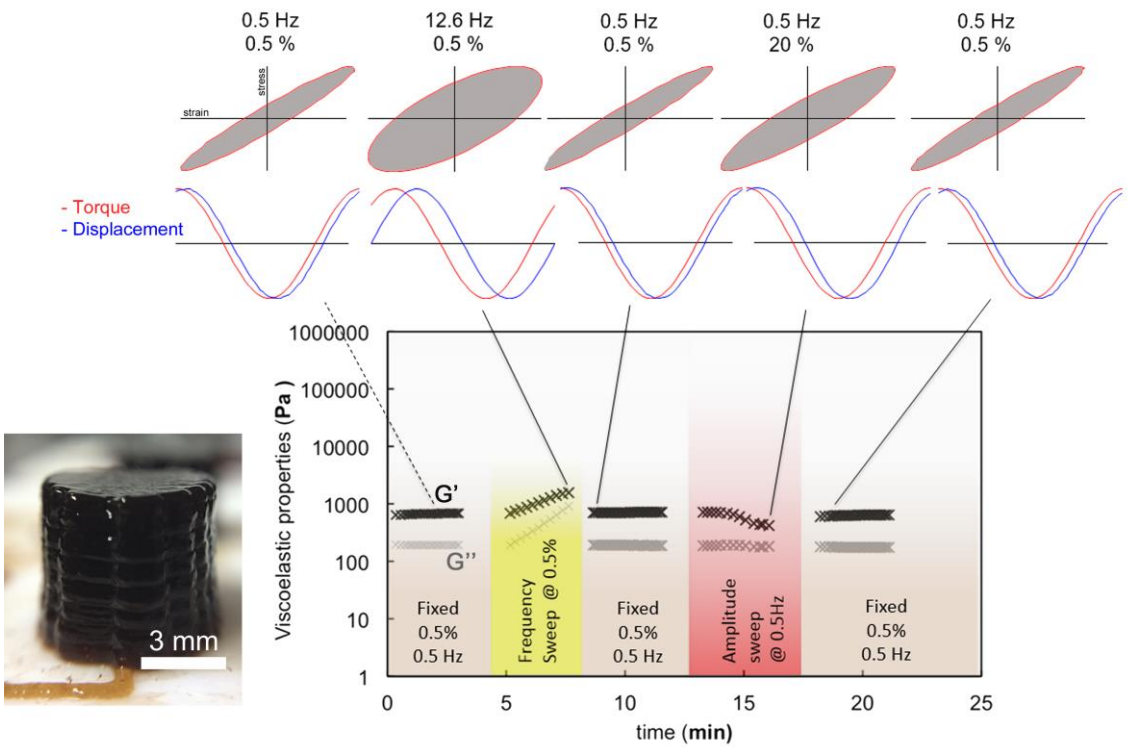

Figure 6. GO aids the printing of PVA solutions. 3D printed PVA-GO cylinder and viscoelastic fingerprints for the PVA-GO paste (8 vol% PVA, 0.3 vol% GO in water). The structure of this paste is very stable (steady G' and G'' values) and has a solid like-structure within the LVR at all times. As frequency increases in step 2, there is a considerable increase of the liquid-like component (see phase between sinusoidal signals and the increase of the area within the ellipsoid in the Lissajous plot), but still the solid-like dominates with linear behaviour. Step 3 shows how the paste immediately recovers its initial structure once the frequency is reduced to 0.5 Hz. The structure does not break down under the amplitude sweep (step 4) suggesting the formation of a true gel between PVA and GO.

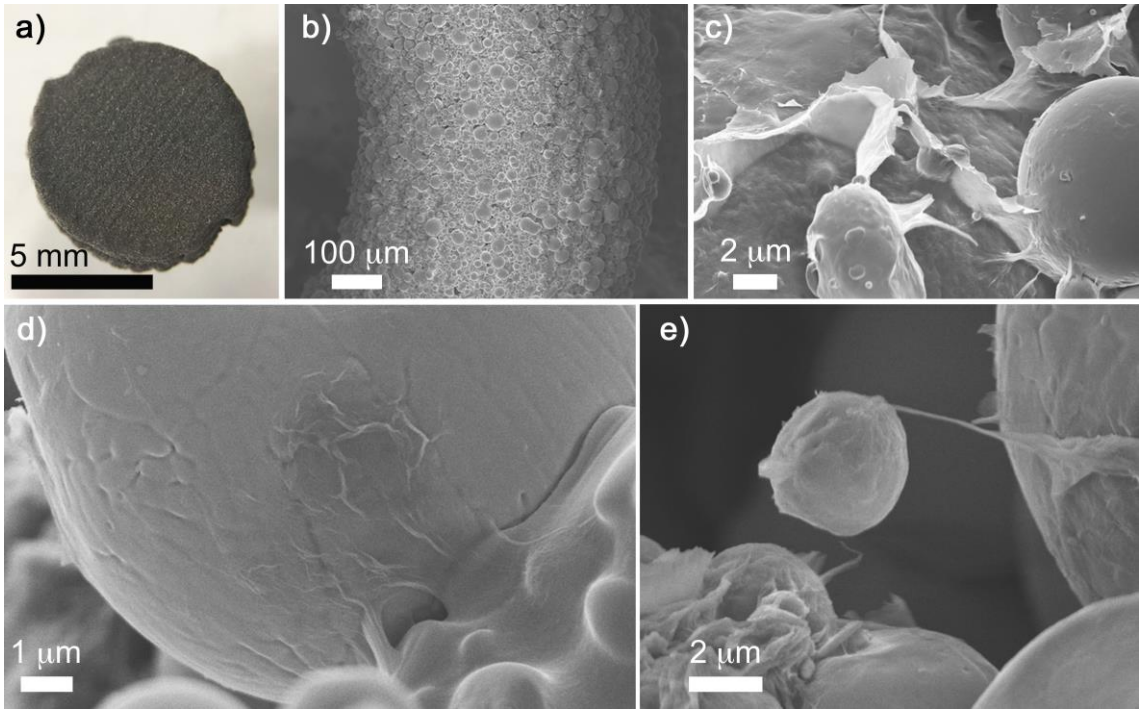

Figure 7. Structural characterisation of 3D printed steel made using GO as printing additive: (a) Image of a steel disc after drying; (b-e) FESEM images at different magnifications. b) External surface of a 3D printed filament where the spheres are evenly distributed bonded by GO. c-e) Morphological details of the GO/steel interactions: GO flakes wrap around the steel particles (c, e) and connect to other particles forming a 3D network. The images (c-e) illustrate this connection, which visually reminds us to the lamellipodia found in cells colonizing surfaces (d). A ~3 μm steel sphere (e) is suspended in an empty space (in a fracture surface) hold by a GO nano scroll that wraps around and connects it to a steel bigger particle.

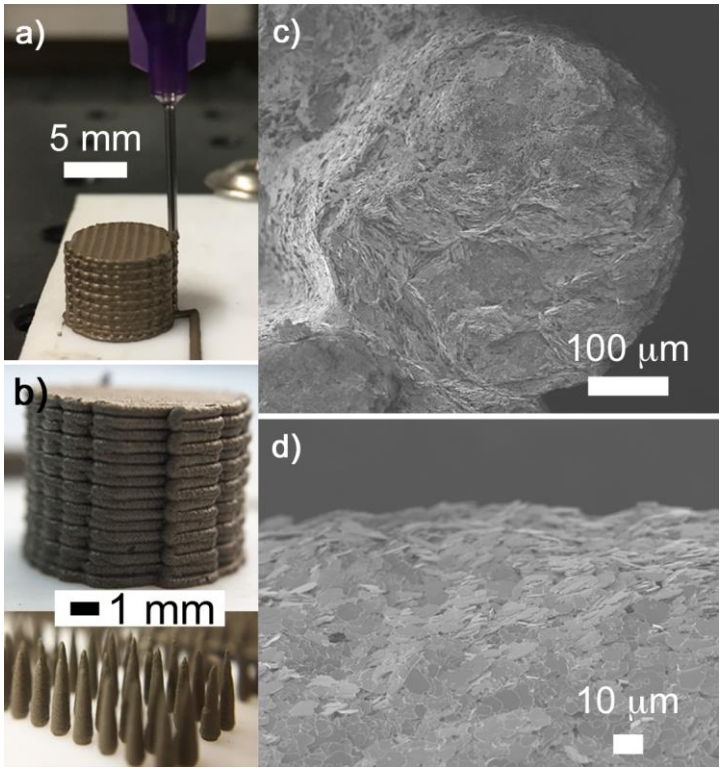

Figure 8. Printing alumina platelets using GO as the only additive: a, b) 3D printed objects (cylinders and micro pillars); and meso scale FESEM images (c, d). c) Cross section of the printed filaments showing domains with random of orientation in the middle; and d) external arrangement of the platelets on the surface of the filament due to the extrusion process.

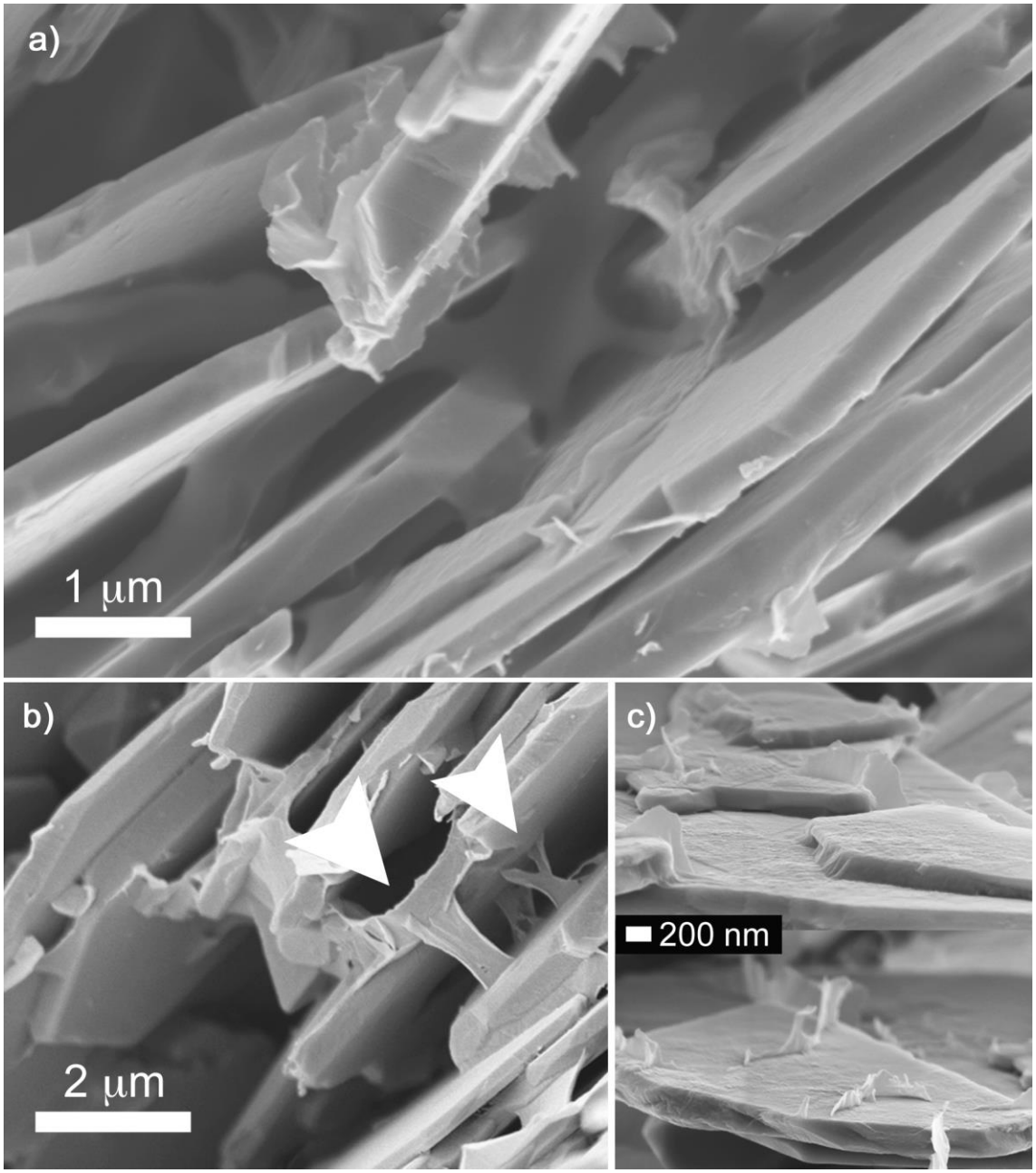

Figure 9. Structural characterization of 3D printed objects made of alumina platelets using GO as printing additive (after drying). FESEM images at the micro and nano scales illustrate the interactions at the GO/platelets interfaces (a, c). A GO flake spreads across and binds multiple platelets (a). GO bridges across platelets highlighted with arrows in (b). GO flakes spread and attach to platelet surfaces showing very good and homogeneous contact (c); some parts of the flakes unfold and reach out towards neighboring platelets, forming a network bond by GO.

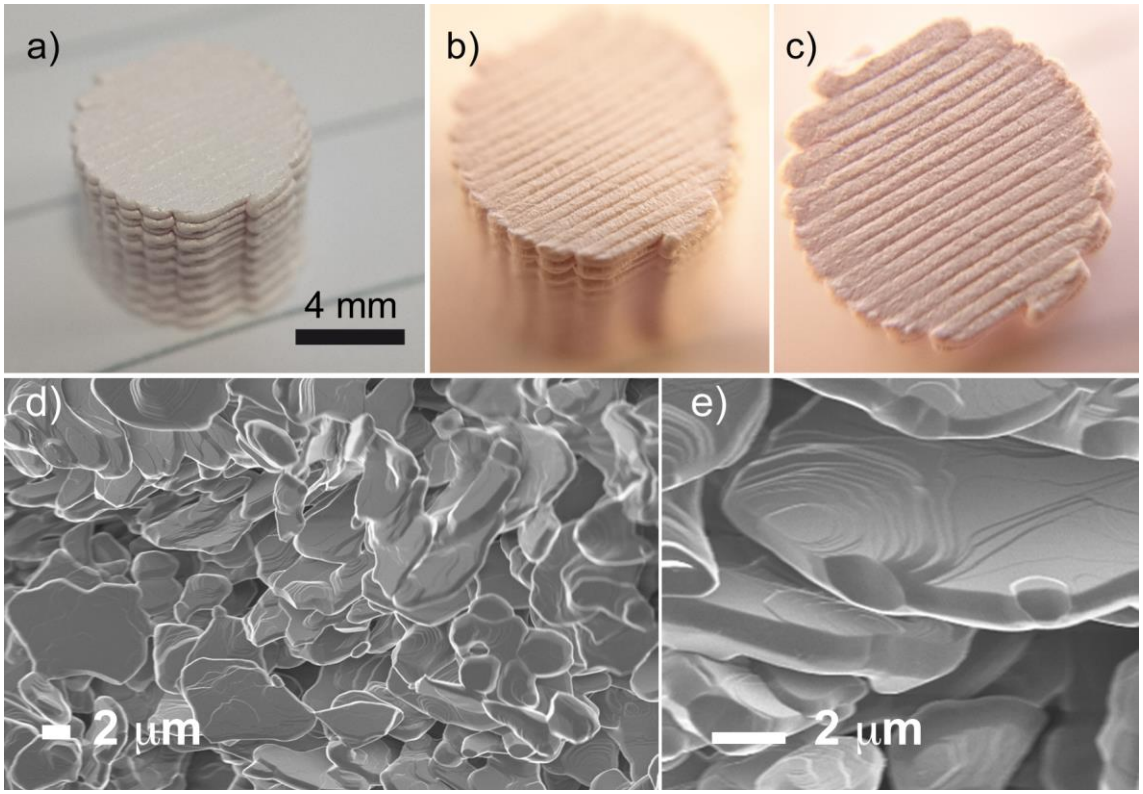

Figure 10. Structural characterisation at multiple scale lengths of a 3D printed cylinder made with an Al_2O_3 platelets/GO paste after sintering at 1550ºC. a-c) Macroscopic images showing the external structure of the cylinder that preserves the morphological features of the printed filaments (side (a), angled (b) and top (c) views). The GO burn out results in a weight loss of ~3 wt%. The bulk volume is subjected to a homogeneous shrinkage of ~4 % after sintering. d, e) SEM images of the internal microstructure with open porosity of 60% calculated using an Archimedes kit. GO also enhances the sintering between platelets (d).

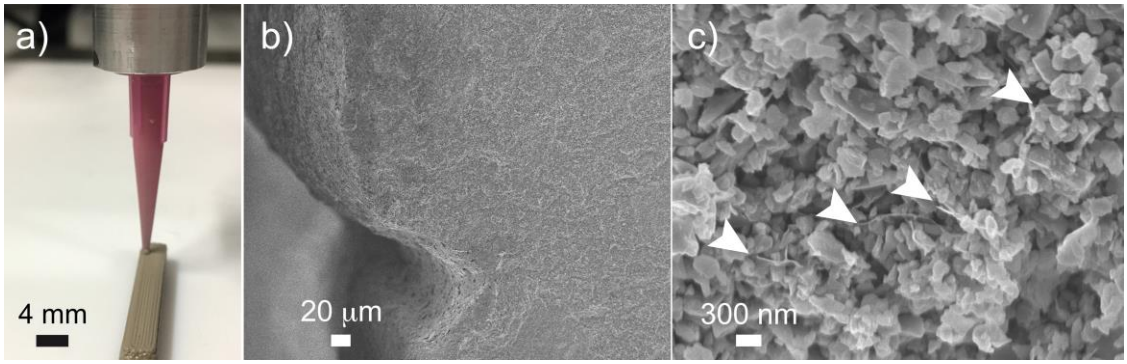

Figure 11. Using GO to aid the printing of SiC objects: a) SiC bar during the printing process; b, c) FESEM images showing the internal structure at the meso and micro scales. The surface of a fractured bar shows a very homogeneous morphology (b) with no pores or gaps between filaments. SiC particles are very small compared to the lateral flake size of GO, making difficult to find fine details of SiC/GO interactions during structural characterisation. GO flakes (highlighted by the arrows in c) are well distributed throughout the cross section (c).

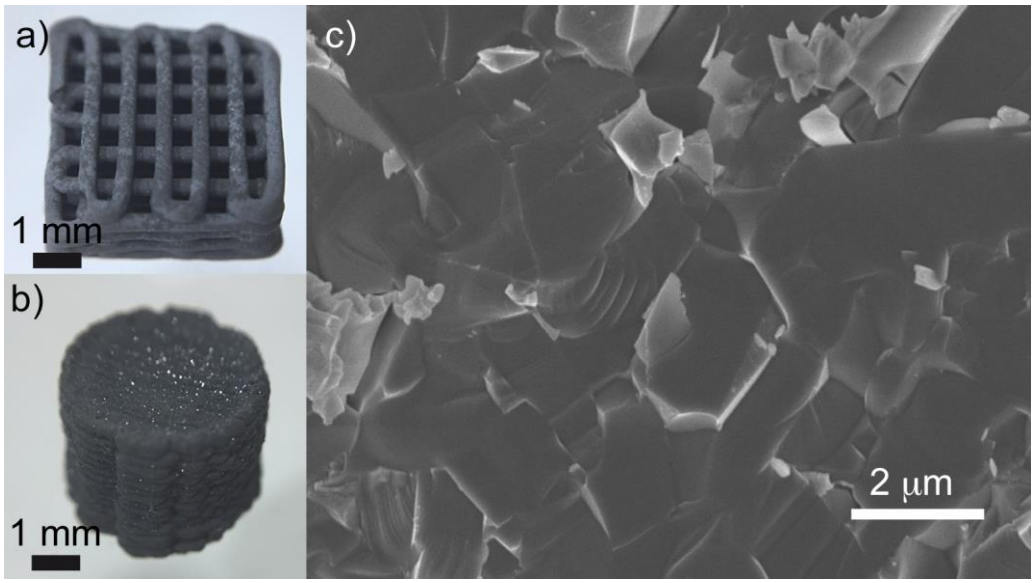

Figure 12. Structural characterisation of sintered SiC structures 3D printed using GO as the only additive. a, b) SiC objects after pressureless sintering under Ar atmosphere at 2050 ºC. c) Fracture surface of a SiC sintered bar (2050 ºC for 2 hours) after mechanical testing showing good density and transgranular fracture. Sintered SiC bars have a final density of 3.21 g/cm^3 (96.4% of the theoretical) and bending strengths of ~212 MPa.

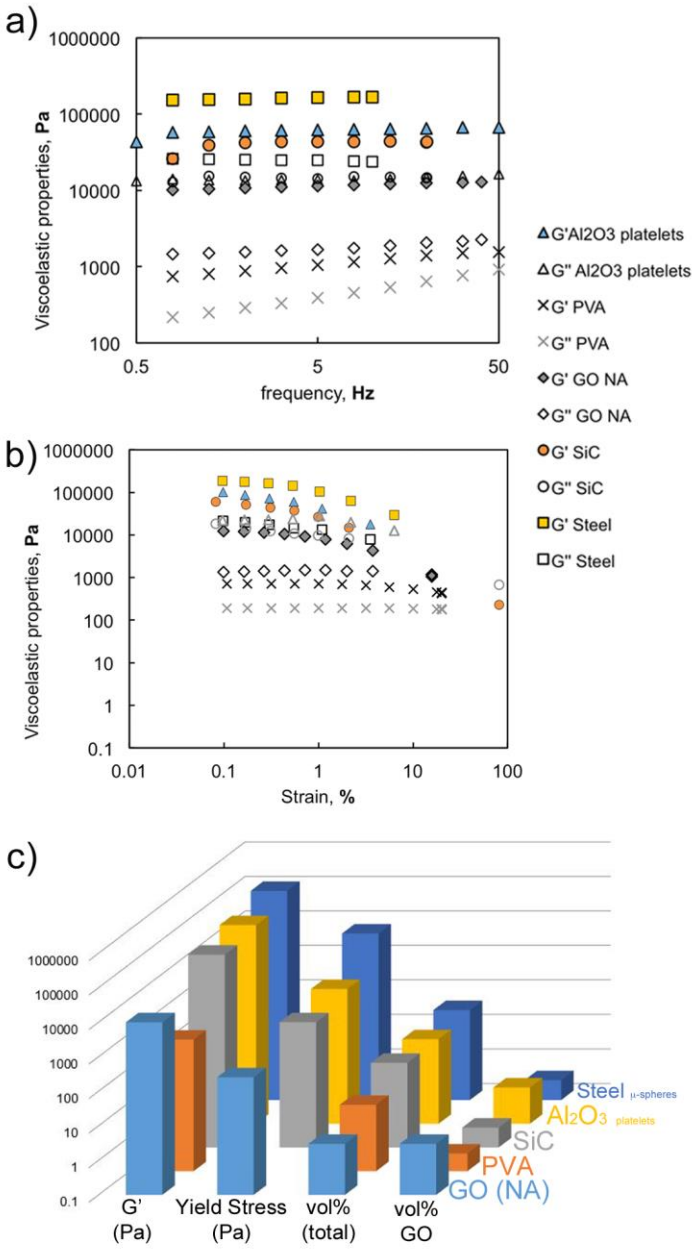

Figure 13. Comparing the viscoelasticity of selected formulations made using GO as the only additive: pure GO (3 vol% GO, 76 mg/mL), SiC powders (0.4 vol% GO, 10 mg/mL), PVA (0.3 vol% GO, 7 mg/mL), Al_2O_3 platelets (1.1 vol% GO, 33 mg/mL) and steel micro-spheres (0.4 vol% GO, 19 mg/mL). Each system has a different response according to the intrinsic properties of the material. The frequency sweep (a) and amplitude sweep (b) provide information of the structure and viscoelastic response that is compiled in (c) for comparative purposes. c) Histogram comparing the viscoelastic properties: storage modulus, G' (obtained from a time sweep at 0.5Hz and 0.5% strain) and yield stress (obtained from b). The chart also displays their total solid loading (vol%) and GO content (vol%). Note that PVA-GO is the only system that forms a true gel; its combined structure does not break down with strain and its behaviour remains within the LVR as strain increases. On the contrary, Steel-GO and ceramics-GO systems break down at strains that range between 3 and >20% depending

on the material (b, c). In general they have an initial linear behaviour before the transition to liquid-like (except for SiC-GO, Figure S3).

TOC graphic